

Reconnaissance Exploration for Gold in the Misaki Area within the Iramba-Sekenke Greenstone Belt, Central Tanzania

Zortosy M. Mpangile^{1,2}, Emmanuel O. Kazimoto^{3*}, and Michael M. Msabi¹

¹Department of Geology, University of Dodoma, Dodoma, Tanzania

²Geological Survey of Tanzania, Dodoma, Tanzania

³Department of Geology, University of Dar es Salaam, Dar-es-Salaam, Tanzania

*Corresponding author, e-mail: ekazimoto@udsm.ac.tz,

Co-authors e-mail: zortosym@gmail.com, mmsabi@yahoo.com

Received 25 Jan 2020, Revised 20 Mar 2020, Accepted 27 Mar 2020, Published 31 Mar 2020

Abstract

Combinations of geological, geophysical and geochemical techniques have been used to explore for gold deposits at Misaki within the Iramba-Sekenke Greenstone Belt in Singida region. The Misaki area is occupied by different rocks including homogeneous coarse-grained granite containing numerous xenoliths (> 5 vol. %), tonalite, K-rich granite, pegmatite and dolerite dykes. All granitic rocks have been intruded by dolerite dykes, cut by epidote veins and are found juxtaposed to a tonalitic rock. Granitic rocks contain mainly anhedral to subhedral K-feldspar, plagioclase, quartz, biotite, hornblende, muscovite and opaque minerals, whereas tonalite contains similar minerals with relatively large amounts of plagioclase and mafic minerals (> 10 wt. %; biotite, hornblende and opaque minerals) and no K-feldspar. The rocks are weakly foliated to massive and poikilitic. K-feldspar is perthitic, whereas plagioclases have cores with rim overgrowths. Chlorite, epidote and sericite in the rock formed at the expense of primary minerals under greenschist facies conditions. Geophysical datasets managed to identify lineaments that crosscut different rocks at Misaki, from which three (3) major structural trends have been recognized, which are NE-SW, NW-SE and ESE-WNW. Results from radiometric data mapped different lithological units by their different radiometric element contents (U, Th and K), distinguishing areas occupied by sediments or sedimentary rocks and those underlain by granitoid rocks. Soil geochemical survey have identified gold anomalies of up to 0.2 ppm Au that in parts show strong affinity with Pb. Bismuth and arsenic were also found to be associated with Au in the soil. Gold anomalies when overlaid with magnetic lineaments indicate an association of gold with NE-SW trending lineaments. Results of this work call for a follow-up detailed geological mapping that would involve trenching and sampling of unweathered rocks, and documentation of geological structures to uncover potential gold deposits of the Misaki area within the Iramba-Sekenke Greenstone Belt.

Keywords: Gold exploration, Iramba-Sekenke, Greenstone Belts, Integrated prospecting

Introduction

Gold deposits in Archean granite-greenstone belts are often hosted but not limited to mafic-ultramafic volcanic rocks or their metamorphic equivalents (Cloutier et al. 2005, Cook et al. 2016, Goldfarb 2005, Henckel et al. 2016, Kazimoto and Ikingura

2014, Sanislav et al. 2015). Other deposits are hosted within intermediate and felsic igneous rocks, sedimentary and metasedimentary rocks (Goldfarb et al. 2005, Henckel et al. 2016, Kazimoto and Ikingura 2014, Kwelwa et al. 2013, Sanislav et al. 2015). Most of these rocks are truncated by regional and

local geological structures, such as faults and shear zones, some of which were conduits for auriferous fluids and sites of deposition of gold and other minerals (Sanislav et al. 2018, Vos et al. 2009). Gold in these deposits occur as nuggets, dissemination within quartz or quartz-carbonate dominated veins, shear zones and within hydrothermally altered rocks. The common known hydrothermal alteration types include silica, potassic, sulphide, sericite and chlorite alteration (Groves et al. 1998, 2003).

Some of the above-described lithological features are important in generating geophysical and geochemical signatures that may be used in exploration for gold deposits within Archean granite-greenstone belts. For example, variations in lithologies such as different mineralogical or geochemical composition, hydrothermal alteration zones and variable weathering intensities, may provide distinctive signatures that are potentially detected by geophysical (aeromagnetic, gravity or radiometric) and geochemical techniques. The use of regional-scale radiometric data can assist in selecting areas with different rocks having high contents of incompatible elements such as U, Th and K, which have also radiogenic isotopes. Moreover, different contents of ferromagnetic and paramagnetic minerals in rocks within or outside gold deposits may assist in distinguishing different lithologies or unmineralised and mineralised vein structures in terrains. Another significance of using these salient mineralogical, petrological, or geochemical signatures of granite-greenstone belt rocks in exploration for gold deposits lies with the fact that most of the areas in tropic countries like Tanzania are covered by overburden or relative young cover rocks. Therefore, exploration activities depend highly on finding the mentioned anomalies in the subsurface by using geophysical techniques, and geochemical analysis for

geochemical signatures in soils or sediments that may be inherited from primary unweathered rocks.

These techniques have been successfully used for many years to locate deposits in different areas of the Tanzania Craton, e.g., North Mara, Geita or Bulyanhulu. Most of the known large-scale gold mines in the Tanzania Craton are so far known from the Sukumaland, Nzega and Musoma- Mara Greenstone Belts (Henckel et al. 2016). Apart from Mwenge and Sambaru-Londoni gold prospects which are locally mined, little is known about gold deposits of the Iramba-Sekenke Greenstone Belt in Singida region. In the present study, integrated analysis of geological mapping, geochemical and geophysical datasets have been applied in order to characterize the geology of the Misaki area, and explore for gold in Misaki within the Iramba-Sekenke Greenstone Belt.

Geological settings of Misaki area

Misaki area is located in Singida region in central Tanzania covering an area of approximately 900 km² and bounded by latitudes and longitudes 5°03'56.60"S to 5°20'14.90"S and 34°00'00.00"E to 34°15'48.60"E, respectively (Figure 1). The area is found within the Tanzania Craton that extends from central to northern Tanzania, south-eastern Kenya to southwest Uganda, and bordered and partly reworked by the Kibaran, Ubendian, Usagaran and Mozambique metamorphic belts (Figure 1). The Craton has been subdivided into three main units: the high grade metamorphic Dodoman Belt, Nyanzian and Kavirondian Supergroups (Pinna et al. 2004; Figure 1). The Dodoman Belt is the oldest (circa > 3.2 Ga) and occupies the lowest position in the stratigraphy. The belt contains high-grade metamorphic rocks including deformed metagranitoids, metavolcanic and metasedimentary rocks.

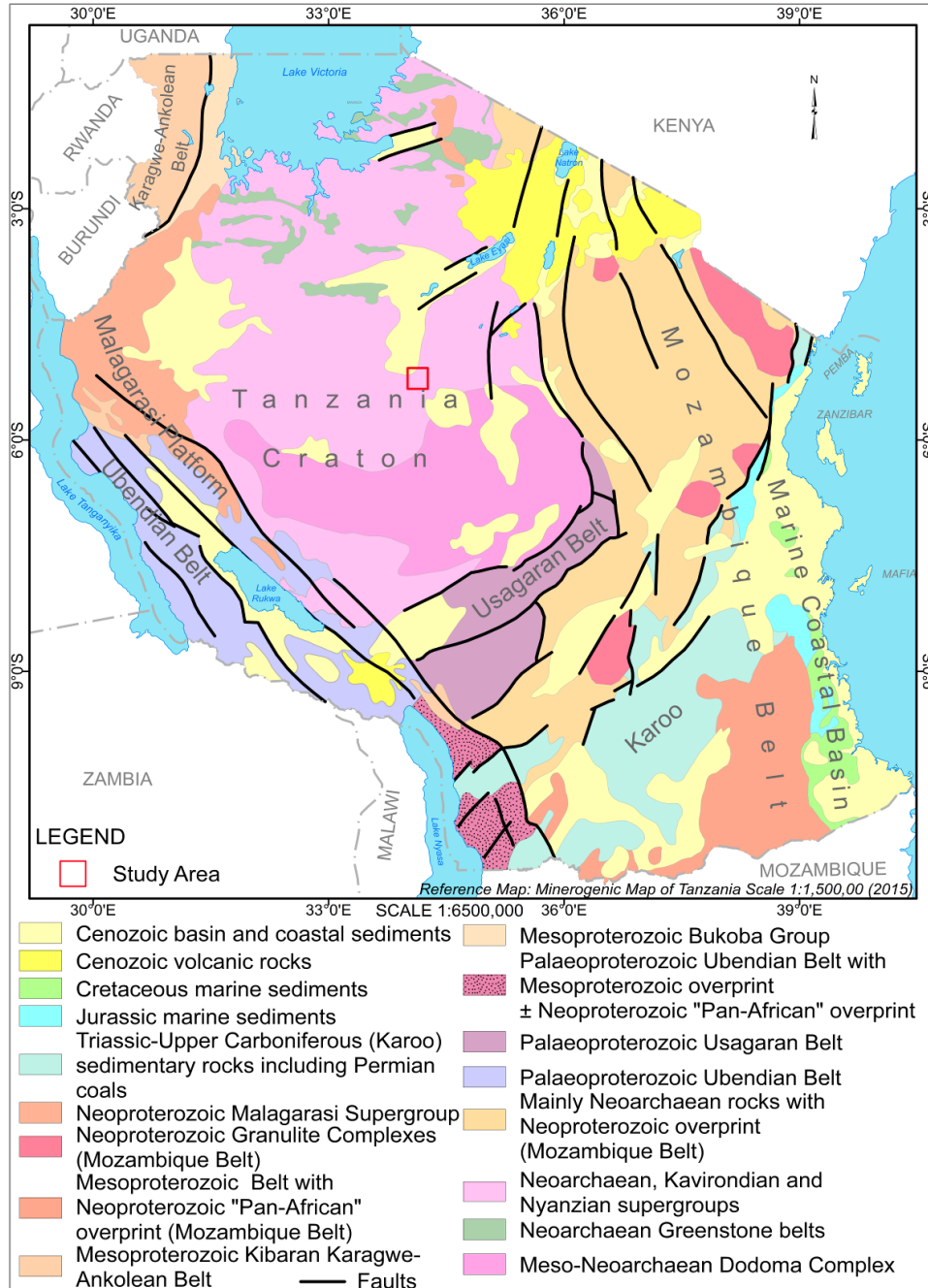


Figure 1: Geological map of Tanzania showing the location of the study area (red box) and major rock units, including Archean Granite-Greenstone Belts (Pinna et al. 2004, Leger et al. 2015).

The Nyanzian Supergroup is subdivided into seven greenstone belts containing granitoid rocks, mafic and felsic metavolcanic rocks interlayered with metasedimentary rocks including Algoma type banded iron formation or ironstones (Borg and Shackleton 1997). The Kavirondian Supergroup is the youngest group of all in the Archean geology of Tanzania. The supergroup mainly consists of sedimentary rocks that in places overlie the rocks of the Nyanzian Supergroup.

The geology of the study area (Figure 2) is presented in QDS 121 that lies within the Iramba-Sekenke Greenstone Belt (Borg and Shackleton 1997) or Manyoni-Moyowosi Superterrane as subdivided by Kabete et al. (2012). The dominant rocks in the study area include grey granite that is cut by young granitoid rocks including granite containing numerous xenoliths of migmatitic biotite and hornblende gneisses and K-rich granite. Other granitoid rocks found in the area are the porphyritic granite and tonalitic rock (Figure 2). These rocks are in parts covered extensively by superficial deposits mainly residual sandy soil and 'mbuga' deposits. To the southwest, the basement cratonic rocks are almost entirely obscured by Kilimatinde Formation, calcrete, conglomerate, sandstone, diatomaceous chert, calcareous mudstone and ferricrete that can reach a thickness of over 30 metres in places. The granitoid rocks are cut by numerous north-easterly striking dolerite dykes. The major geological structures at Misaki and adjacent areas include lineaments or faults, which are prominent and can be observed from aeromagnetic data and Landsat images. Three sets of lineaments in terms of their strike direction, trending NW, NE and ESE can be recognized.

Materials and Methods

Materials

Several field equipment and materials were used during fieldwork in documentation and sampling, including field computer, notebook, Global Position System, geological compass, a geological hammer, digital camera, marker pen and sample bags. Aeromagnetic and radiometric data of Misaki and nearby areas were obtained from the Geological Survey of Tanzania (GST). To accomplish this study, different specialized software including ArcGIS Software version 10.2, QGIS version 2.18 and Oasis Montaj version 8.1 were used in processing images and enhancing or depicting interpreted geological information.

Methods

Fieldwork, thin section preparation, and petrography

Fieldwork involved documentation of lithological units and geological structures, and collecting samples. Rock samples were collected specifically for petrographical studies, whereas soil samples were collected for geochemical analyses of gold and other base metals as indicator and pathfinder elements for gold. All samples were collected in a regular grid pattern with an optimum spacing of 2 km by 2 km between sampling lines and sample sites. Soil was systematically sampled from B-horizon (subsoil) below where organic matter in soil would accumulate for detection of geochemical anomalies (Bradshaw et al. 1979).

Ten representative rock samples were collected for petrographic studies. Thin-section preparation was done following standard thin section preparation procedures at the Geological Survey of Tanzania laboratories. Petrography was done using a standard optical polarization microscope, from which rocks were systematically described in terms of their mineralogical composition and texture.

Geophysical Methods

High-resolution airborne geophysical survey dataset were used to map the subsurface geology and delineate structures beneath the thick regolith in the study area. Geophysical data analysis was done through processing of aeromagnetic magnetic and radiometric data. Both magnetic and radiometric data were processed, gridded and interpolated into regular grid cell for interpretation. Processing of potential field data involved application of various filters that aided interpretation of the subsurface geological features. A regular range of images were used to illustrate the effects of mathematical enhancement techniques which include analytic signal, reduction to pole, first vertical derivative, and tilt angle derivative. The potential data enhancement methods as described by Isles et al. (2013) were applied for enhancing magnetic anomalies of small size and shallow-seated bodies and suppress deeper source in the data. Tilt derivative was applied for deducing the subtle geological boundaries of the various structures enhanced by the other filtered grids. Transformation filters like reduction to pole (RTP) were used to transform magnetic signatures from low magnetic latitude to appear as if the anomalies were obtained at the magnetic poles (Wemegah et al. 2015, Santos and Barbosa 2015).

Radiometric data was processed through various filters and enhancement techniques in order to remove noises to produce a composite image, ratio maps as well as potassium (K), thorium (Th) and uranium (U) maps. A composite image in red green blue (RGB) colour model was created using the Oasis Montaj software package, whereas ArcGIS was used to process, overlay and display the thematic layers. The enhancement of gridded images of potassium (K), thorium (Th) and uranium (U) was performed to interpret radiometric signatures that define lithological units. The ratio images were also created to distinguish lithologies and effects in the data caused by variations in the soil

moisture, non-planar source geometry, and errors associated with altitude correction.

Geochemical analysis of soil and rock samples

Twenty-six (26) soil samples, each weighing 1 to 2 kg, were collected from the Misaki area. Wet soil samples were sun-dried, then broken down and sieved using 2 mm mesh. Each sample was then carefully packed and submitted for analysis at the Geological Survey of Tanzania. At the laboratory, samples were pulverized with a mechanical agate mortar to -75-mesh size and then homogenized. All samples were randomized prior to chemical analysis to avoid any possible systematic bias. Sample analysis was done at the GST, whereby Cu, Ni, Bi, Zr, Zn, As, Pb, and other major elements were determined using X-Ray Fluorescence (XRF). Gold analysis was done using Atomic Absorption Spectrometer (AAS) via aqua regia digestion (Lenahan and Murray-Smith 1986). Samples for gold analysis were weighted up to 50 g and mixed with fluxing agents in crucibles that included lead monoxide (PbO), sodium carbonate (Na₂CO₃), K₂CO₃, silver nitrate AgNO₃, borax glass (Na₂B₄O₇), silica (SiO₂) and reducing agents in different ratios. The sample and flux were then heated to obtain a melt that was left to cool. Lead button was separated from the slag and processed in a separate furnace for a high temperature of about 970 °C for oxidation (cupellation) to form gold prill. Prills were dissolved in a mixture of HNO₃ and HCl (aqua regia) and heated to produce aliquots that were analysed using AAS for their gold contents (Lenahan and Murray-Smith 1986).

Results and Discussion

Rock descriptions and field relationships

Misaki area is covered by young overburden in large part that obscured the field relationship of rocks (Figure 2). Overburden is mainly greyish to brownish sand and silty soil, and gossan. Near to

Mikenene village pebbly sandstone with angular to sub-rounded quartz and iron coated lithic clasts is exposed (Figure 3a). The sandstone is poorly sorted, with clasts supported by rock matrix. On the western part of Misaki occur weakly foliated, medium- to coarse-grained granite that underlies the overburden. Crosscutting the granite are pegmatite and epidote veins, which can be observed in different parts of the Misaki area as well.

The granite contains xenoliths, which were found mainly in its eastern part making more than 5% of the exposed rock (Figure 3b). Xenoliths are of different kinds of rocks, including granitic gneisses, amphibolite and meta-gabbro (Figure 3b). Adjacent to biotite

granite occurs K-rich granite (pink granite; Figure 3c), which is also cut by dolerite and juxtaposed to a tonalite in the eastern and southwestern end of the Misaki area. On the western part and the southwestern end of the Misaki area, porphyritic granite was found, which is medium to coarse-grained. The granite contains large k-feldspar phenocryst making a porphyritic texture (Figure 3d). Relative age relationship between these granitic rocks could not be well established due to limited exposure at Misaki that could reveal their lithologic contact relationship. Moreover, detailed mapping of geological structures was also hindered by the thick overburden.

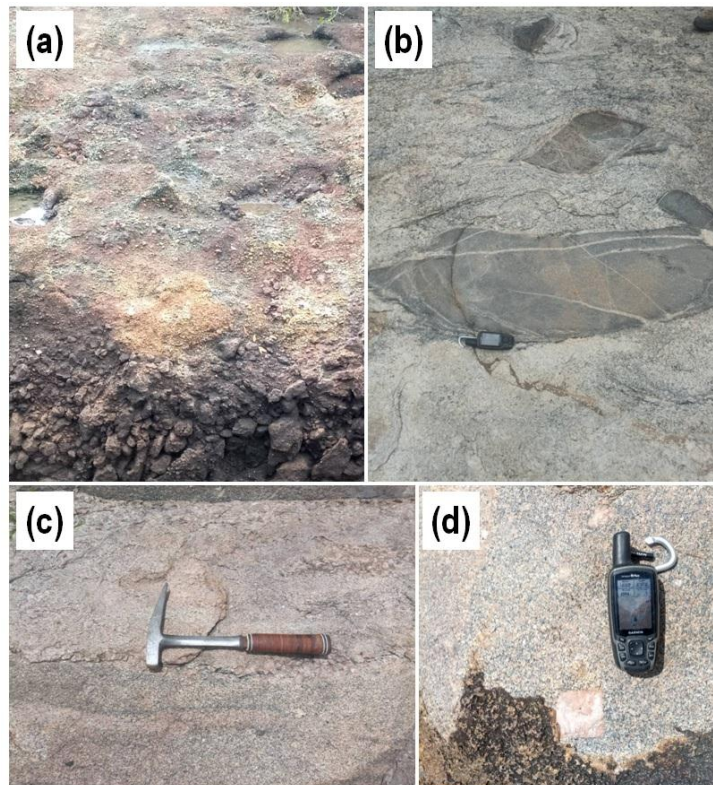


Figure 3: Field photographs of different lithological units at the Misaki area. (a) pebbly sandstone; (b) xenolith-rich granite with amphibolite xenoliths; (c) K-rich granite with pinkish colour due to its high K-feldspar content (microcline); (d) porphyritic granite with large feldspar phenocryst.

Petrography

K-rich granite (pink granite)

Biotite granite is massive and holocrystalline with 90 – 95 vol. % felsic minerals (Figure 4a). The rock is composed of K-feldspar (~45 vol. %), plagioclase (~20 vol. %), quartz (~25 vol. %), biotite (10 vol. %) and minor hornblende and muscovite. Sericite forms as secondary mineral that replaces feldspars. K-feldspar forms perthite, and is poikilitic with inclusions of biotite, quartz and feldspar. Quartz is clear without inclusions but shows undulatory extinction. Biotite is subhedral to anhedral, pleochroic ranging from brownish green, green to light green colour. The crystals have plenty of pleochroic haloes associated with zircon. Plagioclase feldspars is euhedral forming tabular shapes and laths (Figure 4a). The crystals have core and rim overgrowths, in which cores have inclusion.

Porphyritic granite

The rock is weakly foliated with porphyritic texture. It is composed of K-feldspar phenocrysts, plagioclase and quartz, making about 95 vol. % of all minerals in the rock (Figure 4b). The main mafic mineral in the rock is biotite, which is anhedral brownish-green to green coloured. K-feldspar occurs as subhedral to anhedral crystals that form large phenocrysts that are perthitic and poikilitic containing quartz grains. Plagioclase grains have altered to form sericite, whereas chlorite forms at the expense of biotite (Figure 4b). K-feldspar and plagioclase are strongly fractured, whereas quartz shows undulatory extinction (Figure 4b).

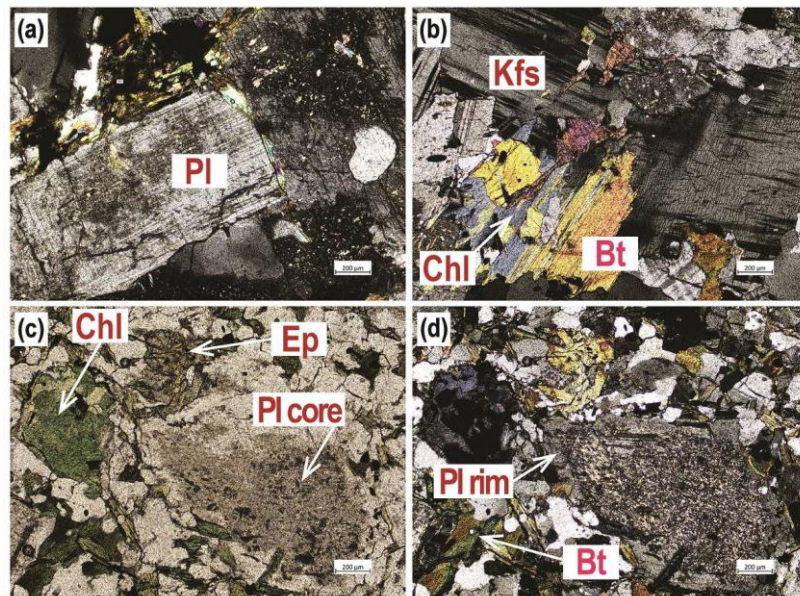


Figure 4: Micrographs of rocks of the Misaki area. (a) Euhedral plagioclase (Pl) lath surrounded by quartz and biotite in biotite granite, and sericite form at the expense of plagioclase; (b) Biotite (Bt), plagioclase, K-feldspar (Kfs) in biotite granite, and chlorite (Chl) forms at the expense of biotite; (c and d) Micrograph of a tonalite observed under transmitted light (c) and crossed polars (d) showing plagioclase with core and rim overgrowth, quartz, epidote (Ep), chlorite (Chl) and biotite (Bt).

Tonalite

Tonalite contains > 85 vol. % felsic minerals. Mineralogical compositions of the rocks include plagioclase (~ 45 vol. %), quartz (20 vol. %) biotite (~ 10 wt. %) and hornblende (2 – 5 wt. %), and no K-feldspar (Figure 4c and 4d). Other minerals in the rocks are epidote, chlorite, calcite and sericite. Accessory minerals are zircon and opaque. Plagioclase is zoned and poikilitic with strongly sericitized cores (Figure 4c and 4d) that encloses inclusions of quartz and biotite. The rims of plagioclase are clear with no inclusions and not sericitized. Biotite forms subhedral to anhedral crystals occurring as laths or flakes in different cut section of a rock. It is zoned with brownish green cores that are surrounded by light green rim overgrowths. Quartz is anhedral, clear without any inclusions, and show undulatory extinction. Epidote and calcite are anhedral formed at the expense of plagioclase, whereas chlorite forms at the expense of biotite and hornblende (Figure 4c and 4d). Sericite formed as secondary mineral after feldspar. The assemblage of epidote, chlorite, calcite, plagioclase rims strongly suggests tonalite metamorphosed under greenschist facies condition.

Grey granite

Grey granite is poikilitic. The rock contains 45 vol. % feldspar, 40 vol. % quartz, 13 vol. % biotite and 2 vol. % opaque phase. Alkali feldspars are perthitic with quartz inclusions. Plagioclase is coarse-grained and anhedral, whereas quartz is colourless and form medium-grained anhedral crystals. Sericite replaces feldspars, whereas iron oxides (hematite?) form along fractures after biotite.

Total magnetic intensity (TMI)

Total magnetic intensity at Misaki revealed four contrasting domains (A, B, C and D) with different magnetic intensities. The first domain in the northern Misaki area, Domain A, is characterised by low magnetic intensities that are below -72 nT, which corresponds to an area occupied by overburden or rocks with low magnetic intensities. Another domain, Domain D, is of moderately high magnetic intensities (-40 to -72) that is underlain by different kinds of granitoid rocks. Domains B and C have both relative high magnetic intensities that range from -40 to 14 nT and from -22 to 63 nT, respectively (Figure 5). These domains are found on where different granitoid rocks are exposed, including xenoliths-rich granite and tonalite.

Magnetic lineaments and geological structures

Total magnetic intensity (TMI) map and other maps derived from applying magnetic filters to TMI are used to reveal magnetic lineaments in the Misaki area (Figure 6). The area has different magnetic lineaments identified by their trends in NW-SE, NE-SW and ESE-WNW directions. These lineaments crosscut each other, and in part their crosscutting relationships can be clearly seen (Figure 6). For example, the NE-SW lineaments are cut and displaced by the NW-SE lineaments, so the latter are younger than the former. By using a First Vertical Derivative (FVD; Figure 7), additional magnetic NE-SW lineaments are identified corresponding to dolerite dykes occurring at the central and southern parts of the Misaki area. The dykes crosscut NNE-SSW lineaments mapped at the southwestern part of the area (Figure 6).

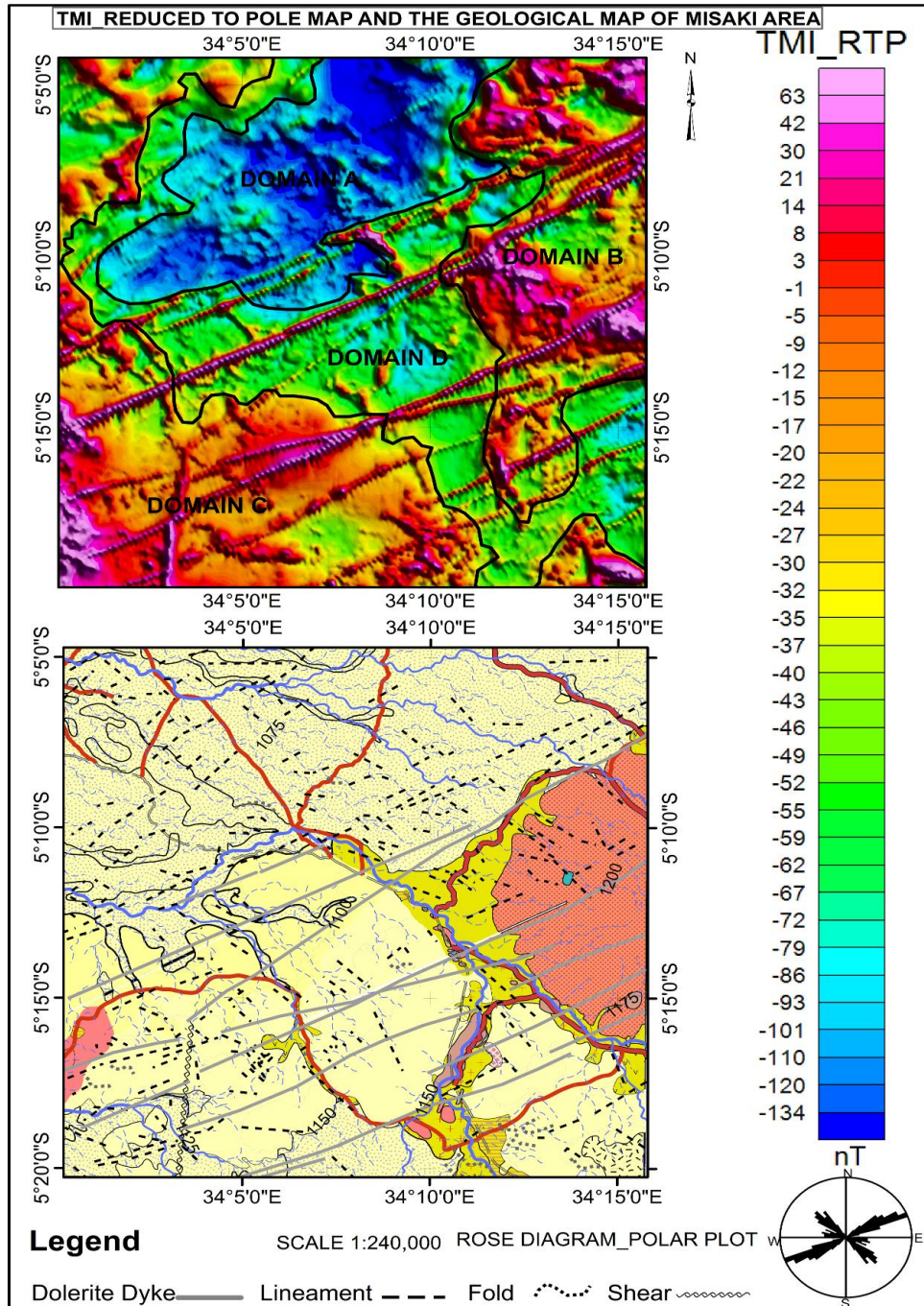


Figure 5: Total magnetic intensity (TMI) map (above), reduced to pole and geological map of the Misaki area (below).

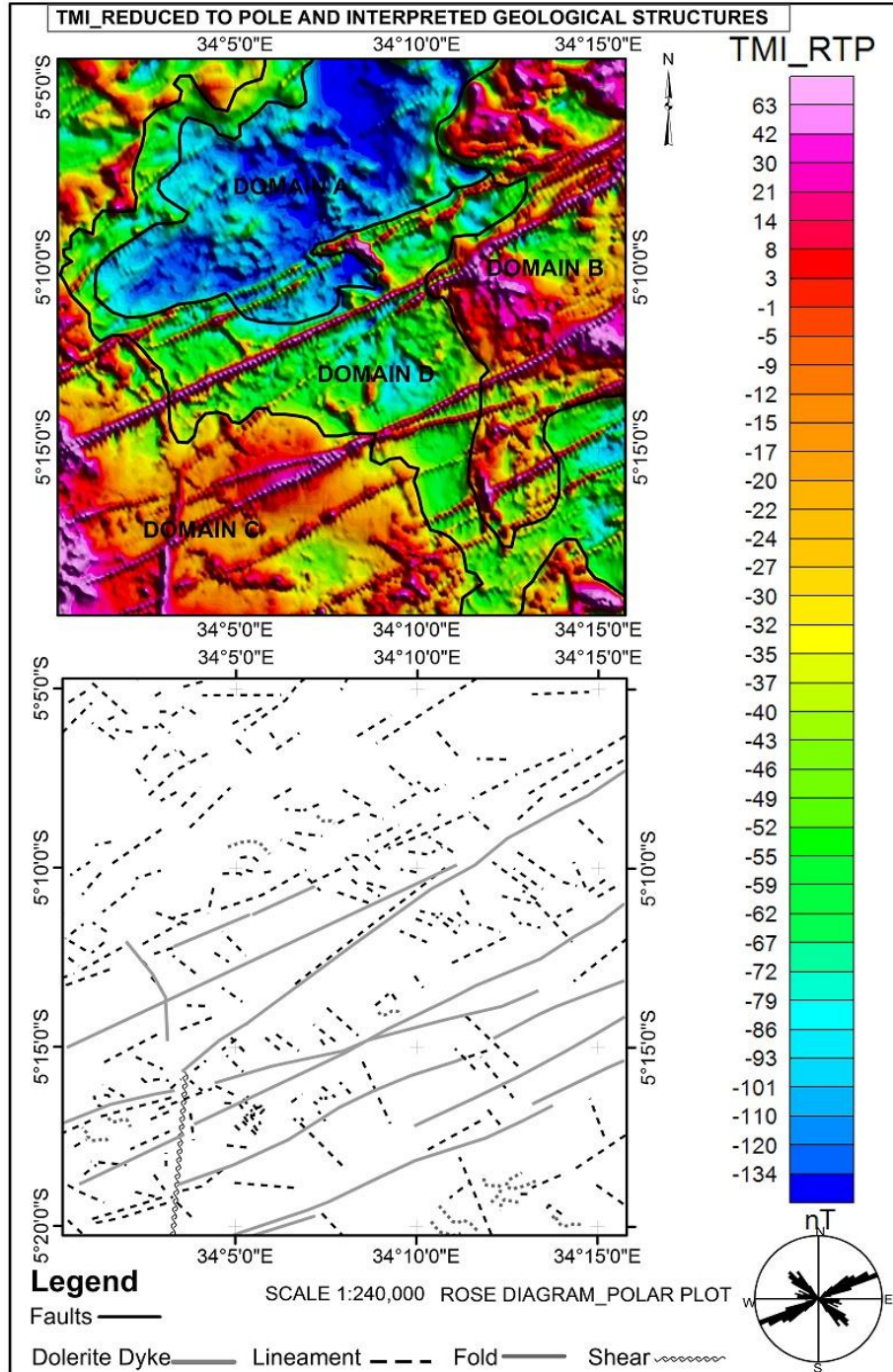


Figure 6: Total magnetic intensity map (above), reduced to pole and interpreted geological structures (below).

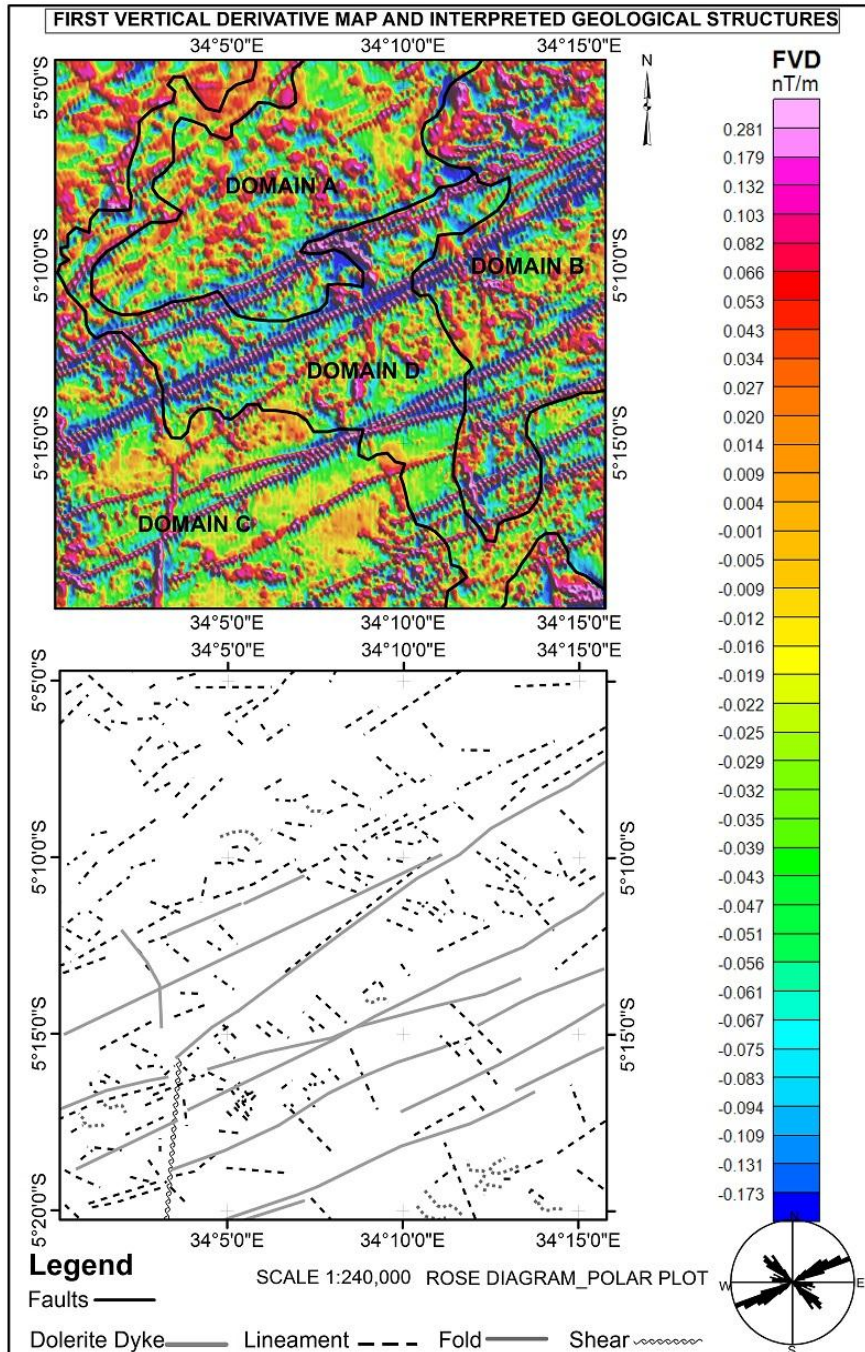


Figure 7: First vertical derivative map (above) and the interpreted geological structures (below).

Interpretation of radiometric data

The high-resolution radiometric data has been used to map superficial cover and different bedrocks basing on their contrasting radioactive element contents (K, Th and U). Polygons A1 - A3 are linked to areas with high K contents, mainly observed in the northwestern western areas (Figure 8). The northwestern, central, eastern, southwestern, and southern areas are associated with both strong Th and U contents (Figure 8), from which by using ratios of Th/K, regions with high-K contents on the northwestern Misaki are clearly mapped, corresponding to Domain A, while those marked as Domain B have low K but relative higher Th content (Figure 8). On the ternary image (Figure 9), relative radiometric intensities related to K, Th and U were assigned red, blue and green colours, respectively. Different rock units can be differentiated from each other by their colour tone from colour composite of red, green and blue image. Some alphabets are assigned to the polygons with similar colour and tones,

thus A1 to A3, B1 to B9, C1 to C7, D1 to D4, E1 to E2 and F1 to F5. The most notable units in the ternary image are appearing in pink and red colour corresponding to K-rich contents (Figure 9).

Granitoid rocks with both K and U contents are shown with magenta. When compared to the existing geological map of QDS 121, areas identified as polygons A and B correspond to outcrops of the granitic rocks (Figure 9). However, polygons B1 and B9 are areas having higher concentrations of K compared to U and Th, which are linked with underlying K-feldspar granite (pink granites). Polygons C1 and C7 are zones with both high K and U correlating with xenoliths-rich granite, whereas polygons D1 to D4 are areas covered by superficial deposits mainly silt, sandy and mbuga soils. Areas with alluvial materials are mapped as polygons E1 to E2 and F1 to F5. These areas have different colour tones caused by their relative concentrations of K, U and Th (Figure 9).

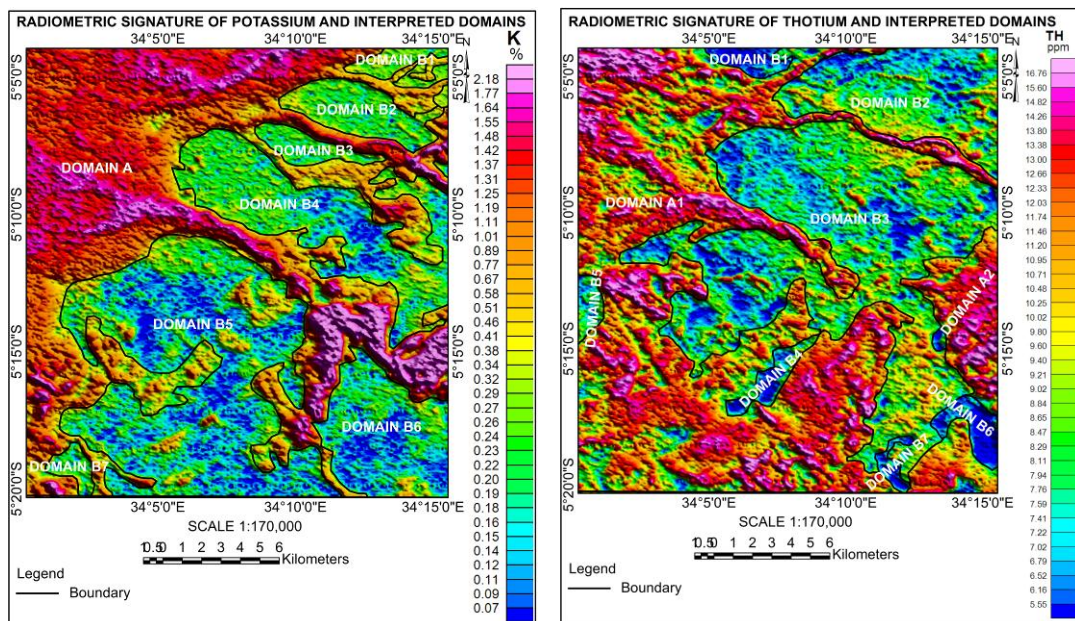


Figure 8: Shows the interpreted lithological units as inferred from the radioelement of potassium, and interpreted lithological domains as inferred from the radioelement of thorium.

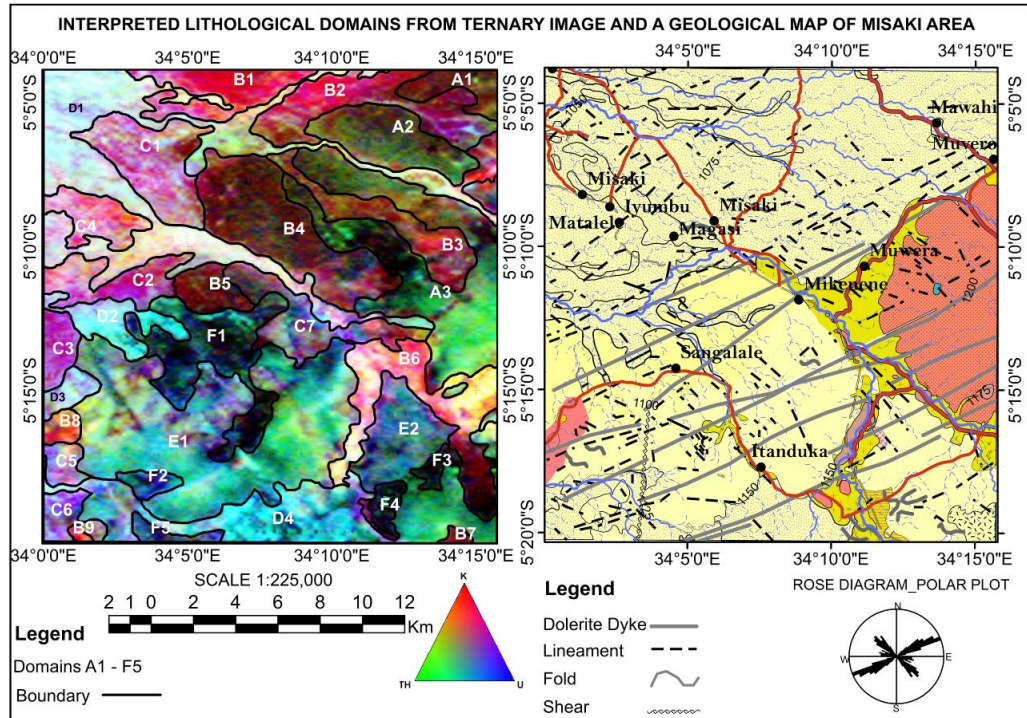


Figure 9: Ternary image for K, Th and U compared with a geological map of Misaki. A1 to A3 and B1 and B9 - (granitic rocks of different types), C1 to C7 and E1 and E2 - (biotite granite with K-feldspar phenocrysts), D1-D4, E1 & E2 and F1 to F5 - (Superficial deposits mainly sand to silt soil and mbuga soil).

Soil geochemical survey results

In order to explore for buried gold deposits underneath the overburden cover, spatial distribution of metals (Au, Pb, As, Cu and Bi) in soil at the Misaki area was determined and shown as Figures 10. Geochemical composition of soil has been presented in Tables 1 and 2. Bubble plots have been used to show different values of gold and gold pathfinder elements. The values of gold in soil have been subdivided into ranges or intervals that the first group of samples has elevated gold contents between 0.17 and 0.21, mainly found in Magasi and Misaki villages, and northeast of Iyumbu and Matalale villages. The next range of gold values is 0.04–0.085 ppm of gold and distributed mainly at Sangalale, north of Misaki and east

of Mikenene village (Figure 2). The third class of gold values is 0.004–0.045 ppm found in the southeast of Magasi, west of Mikenene and northeast of Sangalale villages (Figure 2).

Geochemical distribution map for gold and other metals

The background values for different metals of interest (indicator and pathfinder elements) in soil geochemical survey have been obtained through calculating the mean values and standard deviations, where by anomalous metals values were considered equal to sum of mean and 2 times standard deviation (Sinclair 1974).

Table 1: Major elements compositions (in wt. %) of soil samples from the Misaki area

Sample ID	X	Y	CaO	Fe ₂ O ₃	SiO ₂	K ₂ O	TiO ₂	Al ₂ O ₃	MnO
SSP 001	625396	9426480	0.35	6.58	74.9	1.52	1.34	14.9	0.05
SSP 002	625396	9428480	0.58	7.32	71.6	0.96	1.8	16.6	0.07
SSP 003	625625	9430447	0.32	6.59	74.5	0.73	1.66	15	0.05
SSP 004	627396	9428480	0.33	6.12	78.2	0.72	1.2	12	0.05
SSP 005	627396	9426480	2.22	7.28	83.8	3.78	1.37	<0.01	0.09
SSP 006	619396	9436480	2.08	11.8	66.1	3.53	1.67	13	0.09
SSP 007	625393	9436478	0.65	3.74	91.1	2.99	0.47	<0.01	0.04
SSP 008	627396	9436480	0.72	6.84	87.2	2.92	1.06	<0.01	0.05
SSP 009	625397	9434378	0.86	7.67	87.3	1.68	1.28	<0.01	0.06
SSP 010	629390	9430481	1.22	9.98	75.2	0.66	1.34	10	0.06
SSP 011	631396	9430480	0.43	9.23	87.3	0.51	1.34	<0.01	0.06
SSP 012	627395	9424484	0.35	6.31	77.1	0.66	1.34	13	0.05
SSP 013	619396	9420480	1.37	9.77	74.2	0.11	1.24	12	0.05
SSP 014	623396	9420479	0.41	8.75	87.1	0.44	1.85	<0.01	0.05
SSP 015	623647	9422440	0.56	6.33	82.1	0.15	0.84	9.2	0.03
SSP 016	621397	9422482	1.94	9.66	85.8	0.12	1.28	<0.01	0.05
SSP 017	621398	9420477	1	11.3	84.6	0.58	1.25	<0.01	0.07
SSP 018	621396	9426478	0.39	6.86	89.4	0.66	1.48	<0.01	0.05
SSP 019	623396	9426478	0.3	5.27	79.3	0.55	1.3	12	0.04
SSP 020	623397	9424480	1.73	6.5	81	0.34	0.96	8.5	0.08
SSP 021	637396	9426480	0.23	40.69	57.2	0.27	0.49	<0.01	0.07
SSP 022	636206	9426149	0.34	7.23	75.7	0.32	1.76	14	0.04
SSP 023	627396	9436480	0.28	16.99	70.3	0.3	1.07	10	0.06
SSP 024	635395	9424479	0.97	15.3	63	0.57	2.53	16	0.1
SSP 025	621399	9424479	0.35	6.58	74.9	1.52	1.34	14.9	0.05
SSP 026	619397	9422479	0.58	7.32	71.6	0.96	1.8	16.6	0.07

Table 2: Trace elements compositions (in ppm) of soil samples from the Misaki area

Sample ID	X	Y	Au	V	Cu	Zn	S	Zr	Cr	Ni	Pb	As	Bi
SSP 001	625396	9426480	0.033	40	63	22	147	324	67	45	8	2.815	5.52
SSP 002	625396	9428480	0.029	55	64	22	107	286	75	33	11	2.72	6.60
SSP 003	625625	9430447	0.025	48	78	19	96	271	76	38	11	0.931	6.28
SSP 004	627396	9428480	0.006	52	73	16	161	320	135	52	9	3.267	7.45
SSP 005	627396	9426480	0.028	40	54	23	127	338	74	45	7	3.677	0.1
SSP 006	619396	9436480	0.207	62	76	30	187	324	87	30	25	0.227	22.27
SSP 007	625393	9436478	0.029	25	100	8	253	203	29	48	9	0.6	4.65
SSP 008	627396	9436480	0.013	29	80	15	106	262	81	39	9	4.167	7.70
SSP 009	625397	9434378	0.02	53	76	18	75	303	128	59	15	1.476	8.31
SSP 010	629390	9430481	0.014	49	65	31	14	284	191	57	18	0.657	5.17
SSP 011	631396	9430480	0.017	50	75	16	152	241	132	44	10	1.794	6.51
SSP 012	627395	9424484	0.004	37	74	13	20	327	73	28	10	2.676	5.83
SSP 013	619396	9420480	0.015	50	63	17	126	275	79	37	12	2.96	6.00
SSP 014	623396	9420479	0.007	53	67	16	44	545	78	28	16	3.143	14.70
SSP 015	623647	9422440	0.008	38	51	16	62	199	65	29	12	0.267	7.62
SSP 016	621397	9422482	0.023	49	47	24	202	235	63	42	13	0.1	7.18
SSP 017	621398	9420477	0.017	58	46	17	140	342	76	36	12	1.422	8.30
SSP 018	621396	9426478	0.066	34	52	16	176	326	56	41	11	1.379	0.1
SSP 019	623396	9426478	0.013	54	43	43	200	369	56	34	11	2.096	0.1
SSP 020	623397	9424480	0.004	45	39	19	108	245	40	32	10	2.376	0.1
SSP 021	637396	9426480	0.012	286	83	<0.1	<0.1	229	407	<0.1	15	0.1	0.1
SSP 022	636206	9426149	0.018	62	52	16	56	378	109	30	14	1.237	10.67
SSP 023	627396	9436480	0.012	121	71	24	159	363	156	49	14	3.232	8.95
SSP 024	635395	9424479	0.013	128	37	31	2	552	133	30	18	4.814	19.35
SSP 025	621399	9424479	0.007	60	38	19	<0.1	274	68	30	12	2.741	4.16
SSP 026	619397	9422479	0.004	41	60	22	88	304	66	32	11	18.51	23.01

Anomalous values for an indicator element Au in soil at Misaki were > 0.1 ppm. Gold was found to have a range of concentrations between 0.04 and 0.21 ppm in soil (Figure 10). Elevated values of Au of up to 0.21 ppm (0.17 – 0.21 ppm) were observed in the northern areas near Magasi and Misaki villages and to the northeast of Iyumbu and Matalale villages. Relative lower values than of this first category between 0.04 and 0.09 ppm were observed on the north, at Sangalale and Mikenene village (Figure 2). The remaining areas were found to have Au values between 0.004 and 0.04 ppm, which are considered within background value at Misaki (Figure 10). Common pathfinder elements for Au, like Bi, Pb, As and Cu were also determined. Anomalous Pb content was found to be > 20 ppm, but concentrations in soil were in a limited range between 7 and 25 ppm. Bismuth (Bi) was found to be 0.1 – 23 ppm, with anomalous values > 20 ppm. Anomalous values of Au, Pb and Bi were found to coincide in the eastern, western and northwestern parts of the study area (Figure 10). Arsenic (As) in soil was found to be in a range between 0.1 and 18.5 ppm. Only on western part of Misaki near Sangalale village As was found to be in anomalous > 9.6 ppm (Figure 10). Copper (Cu) anomalies were established at > 94.5 ppm, and actual values in soil were ranging between 37 and 100 ppm. Copper anomaly in soil was found to be located at the northern part of the study area (Figure 10). When overlaid with magnetic

lineaments it appears that gold anomalies associate with NE-SW trending lineaments (Figure 10).

Association of gold and other elements

The nature of associations of elements in soil has been studied through cluster analysis. The data enabled elements to be classified into 5 groups or clusters as follows: cluster 1 with Fe₂O₃, V, Cu and Cr; cluster 2 containing Au, Ca, MnO and Pb; cluster 3 contains SiO₂, S and Ni; cluster 4 have K₂O, and Hg; and cluster 5 contains TiO₂, Al₂O₃, Zn, Zr, As and Bi (Figure 11). Clusters 1, 2 and 5 have different pathfinder elements, which can be described as follows: Cluster 1 can be considered to indicate metals related to scavenging effects of residue Fe³⁺ compounds (von der Heyden and Roychoudhury 2015, Sipos et al. 2014). Second cluster is made of gold (Au) and lead (Pb) that are related with Ca and MnO. This association can be explained if lead (Pb) in the soil is immobile as sulphates or carbonates, in which it associated with Ca in the compounds. Thus, Pb may represent a relic primary dispersion pattern associated with gold. Elements of cluster 3 to 5 may represent residue components of soils, e.g., Al₂O₃ in clays; TiO₂ and Zr in zircon or rutile; SiO₂ in quartz; and As, Bi and Zn as metals scavenged in soils by clays. Although, interpretation of these metal associations would still require further studies on speciation of the metals in soils to ascertain the relationships.

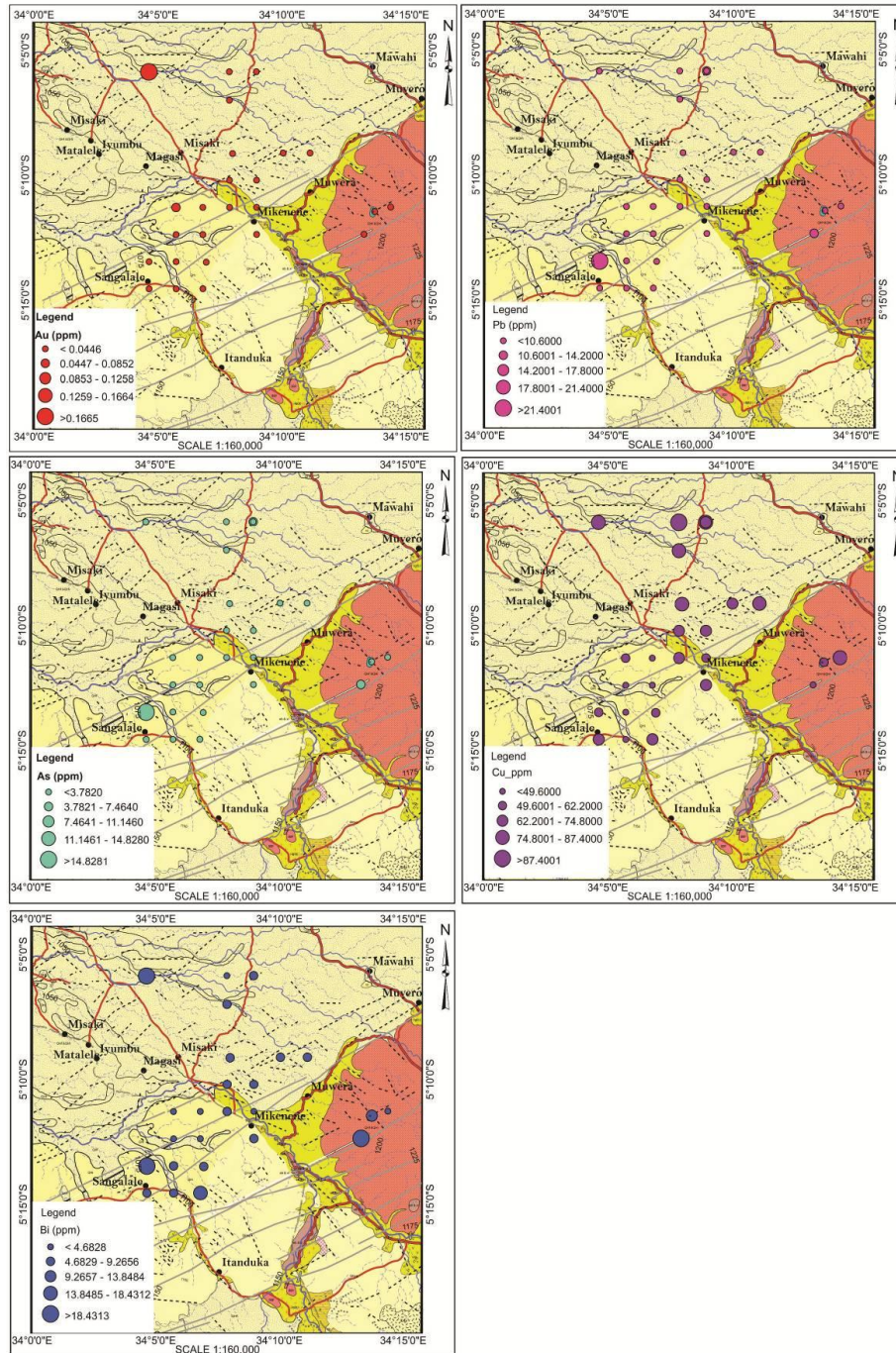


Figure 10: Geochemical distribution map of gold (Au), lead (Pb), arsenic (As), copper (Cu), and bismuth (Bi) in the Misaki area.

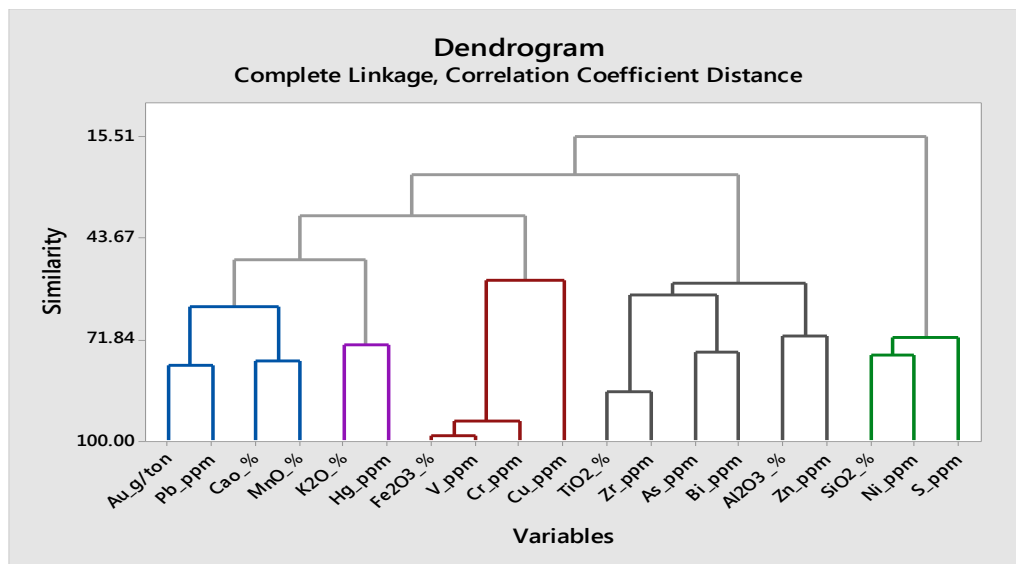


Figure 11: Cluster analysis dendrogram for bulk fraction of soil samples in the study area.

Conclusions

This study employed geological mapping, geochemical and geophysical datasets to enhance the understanding of the geology of the Misaki area and preliminarily explore for gold deposits. Like in any other Archean greenstone terrain of Tanzania, Misaki area has a number of granitoid rocks and several geologic structures of different generations. Geological studies have revealed at least two generations of granitoid rocks that are clearly distinguished by radiometric data: the K-rich granite (pink granite) with high-K content and low Th/K; xenoliths bearing granite that has relative high Th/K (Figures 8 and 9). Xenoliths in the xenoliths-bearing granite reveal different older rocks, including amphibolites and gneisses that were intruded by the granitoid rocks. All these rocks are covered by alluvium and soils in large part of the Misaki area.

The use of geophysical dataset has not only been crucial in geological mapping of the rock units but also in mapping structures buried under overburden cover (e.g., Figure 6 and 7). The granitoid rocks are mapped with relative high total magnetic intensity (TMI)

compared to sediments or sedimentary rocks (Figure 5). Dolerite dykes trending NE-SW and cutting NNE-SSW lineaments have been delineated (Figure 6 and 7). Applications of TMI and various filters to the data enabled identification of magnetic lineaments that are interpreted to represent different geological structures. Analysis of lineaments using a rose diagram revealed three major trends of lineaments dominating at the Misaki area (NW-SE, NE-SW, and ESE-WNW), from which gold anomalies are associated with NE-SW trending lineaments.

Indicator elements in soil have enabled recognition of areas of interest in the north-western parts of Misaki with anomalous gold values of up to 0.21 ppm. Gold in soil has been found to associate with Pb with a close statistical correlation coefficient distance, which is most likely occurring as secondary sulphates or carbonates in soil. Other metals that are associated with gold, although with a distant statistical correlation coefficient have also been detected with values of up to 20 ppm for Bi and 9 ppm for As. Different generations of structures interpreted from magnetic data would require follow up,

especially in areas observed to have anomalous concentrations of both indicator and pathfinder elements for gold.

Acknowledgements

This study was supported by funds from the Geological Survey of Tanzania (GST). The geophysical dataset used in this work was provided by the GST, and is an outcome of World Bank-funded Project involving the GST, British Geological Survey International (BGSi), Council for Geosciences (CGS) South Africa, University of Dar es Salaam, and University of Bergen Norway that was done in the year 2012 and 2013.

References

- Borg GS and Shackleton RM 1997 The Tanzania and NE-Zaire Craton, in: de Wit MJ and Ashwal LD (Eds), *Greenstone Belts*. Oxford University Press: pp. 608–619.
- Bradshaw PMD, Thomson I and Hood PJ 1979 The application of soil sampling to geochemical exploration in non-glaciated regions of the world, in *Geophysics and Geochemistry in the Search for Metallic Ores. Geological Survey of Canada*: pp. 327–338.
- Cloutier JS, Stevenson R, Bardoux M 2005 Nd isotopic, petrology and geochemical investigation of the Tulawaka east gold deposit, Tanzania Craton. *Precamb. Res.* 139: 147–163.
- Cook YA, Sanislav IV, Hammerli J, Blenkinsop TG, Dirks PHGM 2016 A primitive mantle source for the Neoproterozoic mafic rocks from the Tanzania Craton. *Geosci. Front.* 7: 911–926.
- Goldfarb RJ, Baker T, Dubé B, Groves DI, Hart CJR and Gosselin P 2005 Distribution, Character, and Genesis of Gold Deposits in Metamorphic Terranes. *Econ. Geol.* 100th Anniversary vol. 100: 407–450.
- Groves DI, Goldfarb RJ, Gebre-Mariam M, Hagemann SG and Robert F 1998 Orogenic gold deposits: a proposed classification in the context of their crustal distribution and relationship to other gold deposits types. *Ore Geol. Rev.* 13: 7–27.
- Groves DI, Goldfarb RJ, Robert F and Hart CJR 2003 Gold deposits in metamorphic belts: overview of current understanding, outstanding problems, future research and exploration significance. *Econ. Geol.* 98: 1–29.
- Henckel J, Poulsen KH, Sharp T, Spora P 2016 Lake Victoria goldfields. *Episodes* 39: 135–154.
- Isles DJ 2013 Geological Interpretation of Aeromagnetic Data. *The Australian Society of Exploration Geophysicists*.
- Kabete JM, Gorves DI, McNaughton NJ, Mruma AH, 2012 A new tectonic and temporal framework for the Tanzanian Shield: implications for gold metallogeny and undiscovered endowment. *Ore Geol. Rev.* 48: 88–124.
- Kashabano JB, Semkiwa P, Kafumu PD, Mbawala FLK, Mwangosi SA, Shiyoy VL, Mziray AA 2002 Geological map of Misaki (QDS 121). *Geological Survey of Tanzania*. Dodoma, Tanzania.
- Kazimoto EO and Ikingura JR 2014 Trace element geochemistry and petrogenesis of the granitoid and high-K andesite hosting gold mineralization in the Archean Musoma-Mara Greenstone Belt, Tanzania. *J. Afr. Earth Sci.* 91: 66–78.
- Kwelwa S, Many S and Vos IMA 2013 Geochemistry and petrogenesis of intrusions at the Golden Pride gold deposit in the Nzega greenstone belt, Tanzania Tanzania. *J. Afr. Earth Sci.* 86: 53–64.
- Lenahan WC and Murray-Smith RDL 1986 Assay and analytical practice in the South African mining industry. *South African Institute of Mining and Metallurgy, Johannesburg*: p. 616.
- Leger C, Barth A, Falk D, Mruma AH, Magigita M, Boniface N, Many S, Kanya M and Stanek KP 2015

- Explanatory Notes for the Minerogenic Map of Tanzania. *Geological Survey of Tanzania*: p. 376.
- Pinna P, Muhongo S, Mcharo BA, Le Goff E, Deschamps Y, Ralay F and Milesi JP 2004 Geology and mineral map of Tanzania. *Geological Survey of Tanzania*.
- Sanislav IV, Dirks PHGM, Blenkinsop T and Kolling SL 2018 The tectonic history of a crustal-scale shear zone in the Tanzania Craton from the Geita Greenstone Belt, NW-Tanzania Craton. *Precamb. Res.* 310: 1–16.
- Sanislav IV, Kolling SL, Brayshaw M, Cook YA, Dirks PHGM, Blenkinsop TG, Mturi MI and Ruhega R 2015 The geology of giant Nyakanga gold deposit, Geita Greenstone belt, Tanzania. *Ore Geol. Rev.* 69: 1–16.
- Santos MM and Barbosa MSC 2015 Geophysical Analysis Applied to Mineral Exploration in the Region of Morro Do Pilar, Eastern Part of Southern Serra Do Espinhaço-Minas Gerais, Brazil Pp. 1533–38 in 14th International Congress of the Brazilian Geophysical Society & EXPOGEF, Rio de Janeiro, Brazil, 3–6 August 2015.
- Sinclair AJ 1974 Selection of threshold values in geochemical data using probability graphs. *J. Geochem. Explor.* 3 (2): 129–149.
- Sipos P, Choi C, Németh T, Szalai Z and Póka T 2014 Relationship between iron and trace metal fractionation in soils. *Chem. Speciation Bioavailability* 26(1): 21–30.
- Vos IMA, Bierlein FP, Standing JS, and Davidson G 2009 The geology and mineralisation at the Golden Pride gold deposit, Nzega Greenstone Belt, Tanzania. *Miner. Deposita* 44: 751–764.
- von der Heyden BP and Roychoudhury AN 2015 Application, Chemical Interaction and Fate of Iron Minerals in Polluted Sediment and Soils. *Curr. Pollut. Rep.* 1 (4): 265–79.
- Wemegah, DD, Preko K, Noye RM, Boadi B, Menyeh A, Danuor SK and Amenyoh T 2015 Geophysical interpretation of possible gold mineralization zones in Kyerano, south-western Ghana using aeromagnetic and radiometric datasets *J. Geosci. Environ. Protect.* 3: 67–82.